Cellular/Molecular

The R109H Variant of Fascin-2, a Developmentally Regulated Actin Crosslinker in Hair-Cell Stereocilia, Underlies Early-Onset Hearing Loss of DBA/2J Mice

Jung-Bum Shin,[1,2] Chantal M. Longo-Guess,[5] Leona H. Gagnon,[5] Katherine W. Saylor,[1,2] Rachel A. Dumont,[1,2] Kateri J. Spinelli,[1,2] James M. Pagana,[1,2] Phillip A. Wilmarth,[3,4] Larry L. David,[3,4] Peter G. Gillespie,[1,2] and Kenneth R. Johnson[5]

[1]Oregon Hearing Research Center, [2]Vollum Institute, [3]Proteomics Shared Resource, and [4]Department of Biochemistry, Oregon Health & Science University, Portland, Oregon 97239, and [5]The Jackson Laboratory, Bar Harbor, Maine 04609

The quantitative trait locus *ahl8* is a key contributor to the early-onset, age-related hearing loss of DBA/2J mice. A nonsynonymous nucleotide substitution in the mouse fascin-2 gene (*Fscn2*) is responsible for this phenotype, confirmed by wild-type BAC transgene rescue of hearing loss in DBA/2J mice. In chickens and mice, FSCN2 protein is abundant in hair-cell stereocilia, the actin-rich structures comprising the mechanically sensitive hair bundle, and is concentrated toward stereocilia tips of the bundle's longest stereocilia. FSCN2 expression increases when these stereocilia differentially elongate, suggesting that FSCN2 controls filament growth, stiffens exposed stereocilia, or both. Because *ahl8* accelerates hearing loss only in the presence of mutant cadherin 23, a component of hair-cell tip links, mechanotransduction and actin crosslinking must be functionally interrelated.

Introduction

Hair cells of the inner ear detect and transduce mechanical disturbances in the environment, such as sound and head movements (for review, see Gillespie and Müller, 2009). The critical event in mechanotransduction is deflection of the hair bundle, an ensemble of dozens of actin-rich stereocilia projecting from the apical surface of a hair cell. The bundle is held together by extracellular filaments interconnecting stereocilia, including gating elements called tip links (Sakaguchi et al., 2009). Stereocilia are rigid rods that bend at their insertions (Flock et al., 1977), allowing bundle deflections to tension tip links. Elevated tension in tip links, made of cadherin 23 and protocadherin 15 (Sakaguchi et al., 2009), gates transduction channels. For mechanotransduction to be sensitive, stereocilia must be stiff, a feature afforded by abundant actin crosslinkers (Tilney and DeRosier, 1986).

Plastin-1 (PLS1; also known as fimbrin), abundant in intestinal epithelium microvilli (Bretscher and Weber, 1980), was the first actin crosslinker localized to stereocilia (Flock et al., 1982); however, no inner-ear phenotype has been reported in the *Pls1* knock-out (Grimm-Günter et al., 2009). By contrast, the jerker (*Espn^{je}*) mutant mouse completely lacks another actin crosslinker, espin, has very short stereocilia, and is profoundly deaf (Zheng et al., 2000). Espin is not essential for formation of stereocilia but its expression levels control their length (Rzadzinska et al., 2005). Finally, plastin-3 (PLS3; T-plastin) has been reported to appear transiently in stereocilia during development (Daudet and Lebart, 2002). No comprehensive quantitation of actin crosslinkers in stereocilia has yet been performed, however, raising the possibility that other crosslinkers are present.

Mechanotransduction can go awry when key molecules are damaged or suffer from function-altering mutations. Age-related hearing loss (presbycusis) is highly prevalent in human society, reaching half the population by age 80 (Liu and Yan, 2007). Difficult to study in humans because of complex genetics, environmental influences, and slow loss of auditory function, progressive hearing loss arising from genetic causes may be best dissected using inbred strains of mice. Many inbred mouse strains develop age-related hearing loss, and at least nine quantitative trait loci associated with age-related hearing loss have been identified (Noben-Trauth and Johnson, 2009).

The DBA/2J mouse is used widely in hearing research because of its early-onset, progressive hearing loss (Johnson et al., 2008). This mouse harbors both the *ahl* mutation of cadherin 23 (*Cdh23^{ahl}*), which increases the susceptibility to age-related hearing loss in many inbred strains (Noben-Trauth et al., 2003), and *ahl8*, a locus on distal chromosome (Chr) 11 that leads to very-early-onset hearing loss when in combination with *Cdh23^{ahl}* (Johnson et al., 2008). Here we report that the *ahl8*-causative gene is *fascin-2* (*Fscn2*), which encodes an actin crosslinking protein previously thought to be retina specific. FSCN2 is abundant in stereocilia and is developmentally regulated, appearing in inner-hair-cell stereocilia during final stages of elongation. Late

Received March 25, 2010; revised May 7, 2010; accepted June 6, 2010.

This work was supported by National Institutes of Health (NIH) Grants K99 DC009412 (to J.B.S.), R01 DC002368 (to P.G.G.), R21 DC008801 (to P.G.G.), P30 DC005983 (to P.G.G.), and DC005827 (to K.R.J.). The Jackson Laboratory institutional shared services are supported by NIH National Cancer Institute Support Grant CA34196. We thank Beth Burnside for the *Xenopus* anti-FSCN2 antibody and *FSCN2* cDNA and Karen Friderici for the anti-ACTG1 antibody.

Correspondence should be addressed to Peter G. Gillespie or Kenneth R. Johnson at the above addresses, E-mail: gillespp@ohsu.edu or ken.johnson@jax.org.

J.-B. Shin's present address: Department of Neuroscience, University of Virginia, Charlottesville, VA 22908.

DOI:10.1523/JNEUROSCI.1541-10.2010

 0270-6474/10/309683-12$15.00/0

expression and genetic interaction with cadherin 23 suggest that FSCN2 plays a critical role in stabilizing stereocilia after development. Moreover, these results show the power of analyzing complex traits like hearing in inbred strains of mice.

Materials and Methods

Mouse strains and husbandry. All inbred strain mice examined in this study, except for DBA/2NCrl, originated from The Jackson Laboratory. DBA/2NCrl mice were imported into The Jackson Laboratory from Charles River Laboratories International. Experimental mice were housed in the Research Animal Facility of The Jackson Laboratory, and all procedures involving their use were approved by the Institutional Animal Care and Use Committee. The Jackson Laboratory is accredited by the American Association for the Accreditation of Laboratory Animal Care.

Auditory-evoked brainstem response. Hearing assessment was performed as previously described (Zheng et al., 1999). Mice were anesthetized with 2% tribromoethanol (0.2 ml per 10 g of body weight), and then placed on a heating pad in a sound-attenuating chamber. Needle electrodes were placed just under the skin, with the active electrode placed between the ears just above the vertex of the skull, the ground electrode between the eyes, and the reference electrode underneath the left ear. High-frequency transducers were placed just inside the ear canal and computer-generated sound stimuli were presented at defined intervals. Thresholds were determined for a broadband click and for 8, 16, and 32 kHz pure-tone stimuli by increasing the sound pressure level in 10 dB increments followed by 5 dB increases and decreases to determine the lowest level at which a distinct auditory-evoked brainstem response (ABR) wave pattern could be recognized. Stimulus presentation and data acquisition were performed using the Smart EP evoked potential system (Intelligent Hearing Systems).

Scanning electron microscopy. Scanning electron microscopy of inner ear organs was performed essentially as described previously (Furness and Hackney, 1986). Inner ears were dissected out of the skull, fixed in 2.5% glutaraldehyde in 0.1 M cacodylate buffer for 3–4 h at 4°C, and then washed three to four times in 0.1 M phosphate buffer. Hair cells of the organ of Corti were exposed by carefully dissecting away the overlying bone and membrane. Mouse cochleas were processed in osmium tetroxide-thiocarbohydrazide, dehydrated with ethanol, and critical-point dried with hexamethyldisilazane (Electron Microscopy Sciences). Chicken utricles were postfixed in 1% osmium tetroxide, dehydrated in acetone, and critical point dried in liquid CO_2. Samples were mounted onto aluminum stubs and sputter-coated to produce a 10–15 nm gold coat. Samples were examined at 20 kV with a Hitachi 3000N VP scanning electron microscope (mouse cochleas), or at 5 kV with an FEI Sirion Field Emission scanning electron microscope (chicken utricles).

Genotyping the rs26996001 single-nucleotide polymorphism in exon 1 of Fscn2. Genotyping was accomplished by PCR amplification of DNA extracted from tail tips. PCRs were comprised of 100 ng of genomic DNA in a 25 μl reaction volume containing 50 mM KCl, 10 mM Tris-HCl, pH 9.0 (at 25°C), 0.01% Triton X-100, 2.25 mM $MgCl_2$, a 100 nM concentration of each primer (forward and reverse), a 100 μM concentration of each of four deoxyribonucleoside triphosphates, and 1.0 U of TaqDNA polymerase (5 PRIME MasterMix; catalog number 2200100). PCR was performed in a Bio-Rad PTC-200 Peltier Thermal Cycler. Amplification consisted of an initial denaturation at 97°C for 30 s followed by 40 cycles, each consisting of 94°C for 30 s (denaturation), 60°C for 30 s (annealing), and 72°C for 30 s for the first cycle and then increasing by 1 s for each succeeding cycle (extension). After the 40 cycles, the product was incubated for an additional 10 min at 72°C (final extension). PCR products were visualized on 2.5% SeaKem gels (Lonza).

Primer sequences (forward GTGTGGCCTGTGAGATGGAT, reverse GGCTCACACTCAGCAAATGA) were designed to amplify a 216 bp region within exon 1 of *Fscn2* containing the rs26996001 single-nucleotide polymorphism (SNP). Synthesized primers were purchased from Integrated DNA Technologies. To genotype the SNP in DBA/1J, DBA/2JaSmnJ, DBA/2DeJ, and DBA/2NCrl mice, the 216 bp PCR products were purified with the QIAquick PCR Purification Kit (Qiagen) and sequenced, with the same primers used for DNA amplification, on an Applied Biosystems 3700 DNA Sequencer with an optimized Big Dye Terminator Cycle Sequencing method.

A simple SNP genotyping method was developed using the EagI restriction enzyme that alleviated the need for DNA sequencing. When digested with EagI, the 216 bp PCR product from wild-type DNA is cleaved into 121 and 95 bp fragments, whereas the 216 PCR product from DBA/2J DNA remains intact because the EagI recognition sequence (CGGCCG) is destroyed by the G>A SNP variant (CGGCC**A**). After PCR, the reaction mixes were incubated at 37°C for 2 h to overnight with 0.8 μl of EagI restriction enzyme (New England Biolabs). The differently sized EagI-digested PCR products were used to screen progeny of host females implanted with microinjected embryos and identify those with B6-derived *Fscn2* transgenes. This genotyping method was also used to determine the chronology of *Fscn2* SNP variants in DBA/2J strain mice by analysis of archived DNAs. We examined DNA samples from DBA/2J foundation line mice archived in 1985, 1989, 1991, and 1999, and DNA samples from DBA/2J strains with various mutations archived as follows: *ho-4J* (1975), *sdy* (1983), *ge* (1988), *gc* (1988), *pdw* (1991), and *pe-8J* (1992).

Detecting expression of the C57BL/6J-derived Fscn2 *transgene in DBA/2J mice.* Total RNA from kidney, brain, and inner ear was isolated with Trizol reagent following the protocol of the manufacturer (Invitrogen). Mouse cDNA samples were synthesized with the iScript cDNA Synthesis Kit (Bio-Rad Laboratories) and used as PCR templates to assay *Fscn2* expression. Primers (forward GTGTGGCCTGTGAGATGGAT, reverse GTCTCCTGGTCGATTTGCAT) were designed to amplify a 671 nt region extending from exon 1 to exon 2 of the *Fscn2* transcript and containing the rs26996001 SNP. These primers do not amplify a product from genomic DNA because of the large interprimer distance (4778 bp), which spans intron 1. When digested with the restriction enzyme EagI, the 671 PCR product from wild-type C57BL/6J cDNA (which contains two EagI recognition sites) is cleaved into three fragments (353, 223, and 95 bp), whereas the PCR product from DBA/2J cDNA is cleaved into only two fragments (448 and 223 bp), because one of the EagI sites is destroyed by the SNP variant.

*Construction of D2.B6-*ahl8 *congenic lines.* Two congenic lines were constructed by introgression of B6-derived regions of distal chromosome 11 onto the DBA/2J strain background. This introgression was accomplished by repeatedly backcrossing C57BL/6J × DBA/2J hybrids to DBA/2J mice. At each backcross generation (*N*), hybrid mice were selected on the basis of distal Chr 11 marker genotypes. For the "long" congenic line (D2.B6-*D11Mit333-Fscn2*), only mice with B6-derived alleles for *D11Mit333*, *D11Mit203*, and *Fscn2* were selected for backcrossing. For the "short" congenic line (D2.B6-*Fscn2*/Kjn, Jackson Laboratory stock # 12438), only mice with a B6-derived *Fscn2* allele were selected for backcrossing.

Production of DBA/2J mice with C57BL/6J-derived Fscn2 *transgenes.* Purified DNA of BAC clone RP24-180N9 (originally derived from C57BL/6J mice) was obtained from The Jackson Laboratory's Molecular Biology Service and provided to the Cell Biology and Microinjection Service for injections into pronuclei of DBA/2J embryos (0.5 dpc). Two hundred eleven mice were produced from multiple injections and host female implantations and were screened for the *Fscn2* transgene as described above. Two positive carriers were identified and used to establish two separate lines of transgenic mice: line 1, formally designated DBA/2J-Tg(RP24-180N9)1Kjn (stock #12439); and line 2, designated DBA/2J-Tg(RP24-180N9)2Kjn (stock #12440).

Sequencing chicken FSCN2 cDNA. Although the assembled chicken genome contains only 3′ end of FSCN2 (~30% of the total coding sequence), several chicken EST clones (DR426904 and DR425788) contained sequence homologous to the 5′ end of mouse, human, rat, bovine, and *Xenopus* FSCN2 cDNA sequences and were clearly different from FSCN1 and FSCN3. Using a 5′ primer based on the EST sequence (CACCCCAACGAATGGGATCC) and a 3′ primer derived from the database sequence (TCAGTACTCCCAGAGCGTGGC), we amplified the full-length chicken FSCN2 cDNA sequence, confirming the sequence by Sanger sequencing. The accession number is GU907099.

Proteomics analysis. E20 chicken utricles were removed from the skull and dissected in cold, oxygenated chicken saline (155 mM NaCl, 6 mM

KCl, 2 mM $MgCl_2$, 4 mM $CaCl_2$, 3 mM D-glucose, 10 mM HEPES, pH 7.25); otolithic membranes were removed without any enzymatic treatment. Hair bundles were captured in low-melting-point agarose using the twist-off technique (Gillespie and Hudspeth, 1991; Shin et al., 2007). A variant of the GeLC-MS/MS method (Schirle et al., 2003) was used for protein identification. Bundles from 100 chick ears were subjected to SDS-PAGE using NuPAGE Novex Bis-Tris 4–12% gels; however, proteins were run into the gel only ~1 cm. After staining with Imperial Protein Stain (Pierce), the region of the gel with bundle proteins was cut into six equal bands. Each gel slice was washed twice with 50% of 100 mM ammonium bicarbonate (AB)/50% acetonitrile, then once with 100% acetonitrile. The proteins in the gel slices were reduced for 45 min with 10 mM DTT in AB, then alkylated for 30 min with 55 mM iodoacetic acid in AB. Gel slices were washed sequentially with 50% AB/50% acetonitrile, then 100% acetonitrile. After drying the gel slices, they were subjected to overnight digestion at 35°C with 10 ng/μl trypsin (Sigma T6567 proteomics grade, from porcine pancreas, dimethylated) in AB. Peptides were extracted sequentially with ammonium bicarbonate/acetonitrile, 5% formic acid, and 100% acetonitrile. Samples were dried and then resuspended in 5% formic acid before tandem mass spectrometry.

Tryptic digests were injected onto a 1 mm × 8 mm trap column (Michrom BioResources) at 20 μl/min in a mobile phase containing 0.1% formic acid. The trap cartridge was then placed in-line with a 0.5 mm × 250 mm column containing 5 μm Zorbax SB-C18 stationary phase (Agilent), and peptides separated by a 2–30% acetonitrile gradient over 140 min at 10 μl/min using a 1100 series capillary HPLC (Agilent). Peptides were analyzed using an LTQ linear ion trap fitted with an Ion Max Source and 34 gauge metal needle kit (ThermoFinnigan). Survey mass spectrometry (MS) scans were alternated with three data-dependent product ion (MS2) scans using the dynamic exclusion feature of the software to increase the number of unique peptides analyzed.

RAW data from the LTQ mass spectrometer were converted to DTA files representing individual MS2 spectra using Bioworks (version 3.3; Thermo Fisher); DTA files were converted to MGF format using merge.pl (Matrix Science). Peak lists were searched with X! Tandem against the Ensembl database (Ensembl *Gallus gallus*, v53, concatenated reversed sequences and full-length chicken FSCN2 sequence added) with the following parameters: fixed modification, cysteine carbamidomethylation; variable modification, methionine oxidation; one missed cleavage allowed; digest agent, trypsin; refinement modifications, methionine oxidation and N/Q deamidation; no removal of redundant spectra; and parent and fragment ion-mass tolerances of +2.5 to −1 Da and ±0.4 Da, respectively. Custom-designed Mathematica programs were used to carry out isoform resolution and generate intensity-factor calculations. To calculate the relative contributions of PLS1, PLS2, and PLS3, which share several peptides, we weighted the total plastin intensity by the relative numbers of unique peptides identified for each isoform.

Immunocytochemistry. Inner ear tissues from P5, P10, and P30 mice, E20 chicken embryos, and adult *Xenopus laevis* were dissected as for proteomics experiments and fixed for 20 min in 3% formaldehyde in chicken saline. Prolonged fixation (>20 min) of the tissue abolished FSCN2 immunoreactivity, especially in the mouse cochlea. Tissues were blocked in blocking solution (PBS containing 3% normal donkey serum, 1% BSA, and 0.2% saponin) and incubated for 2–3 h with the respective primary antibodies in the blocking solution. For immunolocalization of FSCN2 protein in the mouse cochlea and utricle, we used goat polyclonal anti-FSCN2 antibody from Everest Biotech (catalog number EB08002) (5 μg/ml). Polyclonal rabbit antibodies specific for the chicken FSCN2 protein were generated by simultaneously injecting the following peptides into rabbits: CQDEADSSVVFLKSH (#35), CADSELVLRATLWEY (#36), CYTLEFKAGKLAFKD (#37), and CGKNGRYLRGDPAGT (#38). Antibodies specific for each of the peptides were then separately purified with peptide-specific affinity columns. All four of these antibodies worked well in immunocytochemistry and immunoblot experiments. The rabbit polyclonal anti-*Xenopus* FSCN2 antibody was described previously (Lin-Jones and Burnside, 2007). Similar results were seen with a rabbit polyclonal generated against CKEASLPLPGYKVRE (#74). The rabbit polyclonal anti-ACTG1 antibody was described previously (Belyantseva et al., 2009). After primary antibody incubation, tissues were washed with PBS (3 × 5 min) and incubated with Cy5-labeled donkey anti-rabbit or donkey anti-goat secondary antibody (5 μg/ml). FITC-phalloidin (1 μM) was added to visualize actin. After washing 3 × 5 min, tissues were mounted on glass slides in Vectashield mounting medium (Vector) and covered with #1.5 coverslips, using a cut #1 coverslip as spacer to prevent tissue compression. Images were obtained on an Olympus Fluoview 1000 confocal microscope.

In triple labeling experiments, we used FSCN2 antibody #38 and mouse monoclonal 3G10 from Abnova. For profiling FSCN2, PLS1, and actin staining, 14 bundles from three E21 utricles were used; these utricles were folded so the bundles were seen in profile in the confocal microscope. We excluded bundles for analysis that were not fully captured within the stack, as well as bundles lacking PLS1 or FSCN2 and those without a clear cuticular plate to align. We used ImageJ to generate maximum projections; from these images, we captured fluorescence profiles in all three channels that included approximately half the width of the cell and spanned the cell body and bundle. Actin peaks associated with the cuticular plate were aligned in Excel (Microsoft); we used data from that point to the tip of the bundle. Because the actin profiles aligned very well for all bundles, we did not adjust the profiles to make all bundles the same length. To find relative fluorescence, we divided the PLS1 or FSCN2 intensity by the actin intensity at each point; we normalized actin to its peak fluorescence for each bundle, and did the same for PLS1/actin and FSCN2/actin ratios. Averages ± SEM were plotted.

Immunogold electron microscopy. E20 chicken utricles were dissected as for proteomics experiments. Utricles were fixed at room temperature for 30 min in 3% formaldehyde (Electron Microscopy Sciences) prepared in chicken saline, in the presence of 10 μM phalloidin (Invitrogen). Utricles were permeabilized and blocked for 2 h at room temperature in 3% donkey serum (Jackson ImmunoResearch), 2% Fraction V BSA (Calbiochem), 0.2% saponin, 10 μM phalloidin, in 1× PBS (132 mM NaCl, 2.7 mM KCl, 4.3 mM Na_2HPO_4, 1.4 mM KH_2PO_4, pH 7.3). The utricles were incubated overnight at 4°C with anti-FSCN2 #36 at 10 μg/ml in block (3% donkey serum, 2% BSA, 10 μM phalloidin, in 1× PBS). Tissues were washed 3 × 10 min in PBS, then fixed again with 3% formaldehyde and 0.1% glutaraldehyde (Ted Pella) in PBS for 30 min at room temperature; tissues were then washed 3 × 5 min in PBS.

Utricles were incubated for 48 h at 4°C with goat anti-rabbit-10 nm gold (Ted Pella), diluted 1:10 in block (3% donkey serum, 2% BSA, 10 μM phalloidin, in 1× PBS). Tissues were washed 3 × 5 min in PBS and 1 × 5 min in 0.1 M cacodylate, pH 7.4 (EMS), then fixed again for 30 min with 2.5% glutaraldehyde, 1% tannic acid (EMS), in 0.1 M cacodylate, pH 7.4; tissues were then washed in cacodylate, pH 7.4. Utricles were postfixed with osmium (Polysciences) for 1 h at room temperature (1% osmium in 0.1 M cacodylate buffer, pH 7.4); tissues were then washed in cacodylate, pH 7.4.

Utricles were dehydrated at room temperature with acetone (EMS) for 15 min at each acetone concentration (50%, 70%, 95%, 100%). The tissues were transitioned into epoxy (~55% Araldite 502, 44% DDSA, 1% DMP-30; EMS) by incubating them with 1:1 acetone/epoxy for 30 min at room temperature, 1:3 acetone/epoxy for 30 min at room temperature, followed by 100% epoxy at room temperature for 2 d. Utricles in epoxy were then heated at 60°C for 48 h.

Thin sections were cut on a Sorvall MT2-B Ultra Microtome, and mounted on 200 square mesh, thin bar, high-definition copper grids (Polysciences). Sections were stained with uranyl acetate (EMS) for 30 min at room temperature, rinsed with warm, distilled water, and stained with lead citrate (EMS) for 10 min at room temperature, followed by a final rinse with distilled water. Sections were viewed on a Philips CM100 transmission electron microscope.

Immunoblotting. Isolated bundles, still embedded in agarose, and the other tissues were homogenized in reducing SDS-PAGE sample buffer, boiled for 5 min, and microcentrifuged for 5 min to remove insoluble debris. Proteins were resolved using a Bis-Tris SDS PAGE gradient gel (Novex 4–12%, Invitrogen), transferred to PVDF membranes, and stained with India Ink. Blots were then blocked in blocking buffer for 1 h and probed with #36 rabbit polyclonal anti-FSCN2 antibodies for 2–3 h. After 3 × 5 min washing in PBS/0.3% Tween 20, blots were incubated

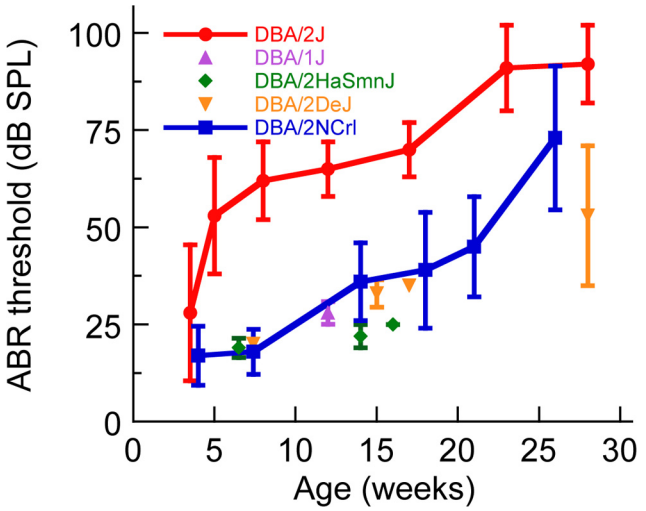

Figure 1. Rapid progression of hearing loss in DBA/2J mice. Average 16 kHz ABR thresholds are shown for five DBA-related strains tested from 4 to 28 weeks of age. The data points for DBA/2J and those for DBA/2NCrl, the most closely related strain, are connected by lines to contrast the difference in their hearing loss progression. Error bars represent the SDs of the means to illustrate the degree of variation observed at each time point. ABR thresholds for all auditory test stimuli, SEs, and numbers of mice tested for each strain and test age combination are given in supplemental Table 1 (available at www.jneurosci.org as supplemental material).

with HRP-conjugated goat anti-rabbit secondary antibody for 1 h, and bands were visualized by ECL reagent.

Quantitative RT-PCR. The entire temporal bone (containing cochlea, otolith organs, and semicircular canals) was dissected from P5, P12, and P30 C57BL/6 mice. For each age, quadruplicates were prepared, each consisting of five temporal bones. Total RNA was isolated using TRIzol reagent (Invitrogen); 1 μg of total RNA was used for the reverse transcriptase reaction using the Bio-Rad iScript kit. The resulting cDNA was diluted 1:200 to be used as template for the qPCR.

Primers were designed using Primer3 (http://primer3.sourceforge.net/); PCR was performed using iQ SYBR Green Supermix (Bio-Rad) with a DNA Engine Opticon System (MJ Research/Bio-Rad). We measured Ct for transcripts of interest and normalized it to Ct for *Gapdh* transcripts. We chose *Gapdh* as the anchor gene as its Ct was relatively stable over the three different ages. Two technical replicates of each of the four biological replicates were carried out.

The following primers for qPCR were used: *Gapdh*: left, CTTCCGTGTTCCTACCCCCAATGT; right, GCCTGCTTCACCACCTTCTTGATG. *Actb:* left, GGGCTGTATTCCCCTCCATCGT; right, CTTCTGACCCATTCCCACCATCAC. *Actg1:* left, GCTATGTTGCCCTGGATTTTGAGC; right, GGAAGGAAGGCTGGAAGAGTGC. *Pls1:* left, CAAGTTCTCTTTGGTTGGCATCG; right, GGGTAAGTGTTGCGTTCCCTTCAT. *Fscn1*: left, GTTTGTGACCGCCAAGAAAAATGG; right, GAAGAGTTCCGAGTCCCCTGCTGT. *Fscn2:* left, CCTCATTTTCCAGAGCAGGCGGTA; right, GGGCTTCAGGTTCCCAGACAAGG.

Results

DBA/2J mice have an early-onset hearing loss and loss of hair bundles

We assessed hearing in DBA/2J and other DBA strain mice by ABR threshold measurements. DBA/2J mice undergo a progressive hearing loss that occurs much earlier and is more profound than in other DBA strains, including the closely related DBA/2NCrl strain (Fig. 1). By 5 weeks of age, the 16 kHz ABR thresholds of DBA/2J mice are already on average 35 dB above those of the normal thresholds exhibited by all other DBA-related strains at that age.

To identify pathological correlates of this hearing loss difference between DBA/2J and DBA/2NCrl mice, we examined cochlear hair cell morphology by scanning electron microscopy (Fig. 2). Hair bundles of DBA/2J mice appeared normal at 2 weeks of age (Fig. 2*a*) but then were progressively lost between 1 and 6 months of age (Fig. 2*b–d*), similar in time course to the loss of function determined by ABR. Bundle loss occurs first near the base of the cochlea and then spreads apically, corresponding with the onset times of hearing loss from high to low frequencies, typical of age-related hearing loss; degeneration occurs first in outer hair cells and later in inner hair cells. Individual stereocilia within a hair bundle show varying degrees of degeneration (Fig. 2*b–e*). In contrast to DBA/2J, bundle loss in DBA/2NCrl mice occurs at much older ages (Fig. 2*h*), consistent with the later onset of hearing loss in these mice (Fig. 1). These results show that *ahl8* produces a rapid hearing loss that is followed by loss of stereocilia and eventual hair-cell degeneration.

DBA/2J mice have a mutation in the *Fscn2* gene

We previously mapped *ahl8* by linkage analysis of (DBA/2J × C57BL/6J) × DBA/2J backcross mice (Johnson et al., 2008). The large effect of *ahl8* on ABR thresholds of these mice (LOD>50) enabled us to refine the candidate gene interval to an 8 Mb region on distal Chr 11 (position 114–122 Mb, NCBI build m37). Because DBA/2J is the only strain surveyed that shows an *ahl8*-influenced hearing loss, we searched SNP databases to identify DBA/2J-specific DNA variants within the *ahl8* candidate interval that are predicted to cause nonsynonymous codon or splice-site changes. Only a single SNP (rs26996001) meeting these criteria was found (Fig. 3*a*), located in exon 1 of the fascin-2 gene (*Fscn2*). We considered *Fscn2*, which encodes an actin-bundling protein (Lin-Jones and Burnside, 2007), to be a plausible candidate gene for *ahl8* because of its potential effect on the strength, flexibility, or dynamics of the actin-filled stereocilia of hair cells.

The DBA/2J variant of *Fscn2* is not found in any of the other 20 inbred strains examined, including the closely related DBA/1J, DBA/2HaSmnJ, DBA/2DeJ, and DBA/2NCrl strains (Fig. 3*a*), none of which exhibit early-onset hearing loss (Fig. 1). The known genealogy of these DBA-related strains (Fig. 3*c*) and genotyping analysis of archived DBA/2J DNA samples indicate that the *Fscn2* G>A mutation occurred in the DBA/2J lineage between 1951 (when it was separated from the DBA/2N lineage) and 1975 (date of the oldest archived sample of DBA/2J DNA).

The DBA/2J variant is predicted to cause a nonsynonymous amino acid change of arginine to histidine at position 109 (R109H) of the mouse FSCN2 protein (Fig. 3*b*). This arginine is conserved in orthologous fascin proteins of all vertebrate species examined and in the paralogous fascin-1 (FSCN1) and fascin-3 (FSCN3) proteins of all mammalian species examined, indicating a constrained functional importance for this residue (Fig. 3*b*). Examination of the structure of closely related FSCN1 (Protein Databank Structure 1DFC) indicated that R109 is located on the surface of the fascin molecule, in a location that could plausibly be involved in binding actin filaments (Fig. 3*d*).

To see whether the hearing loss and *Fscn2* DNA differences between DBA/2J and DBA/2NCrl mice genetically cosegregate, we analyzed ABR thresholds and *Fscn2* genotypes of F2 intercross progeny from (DBA/2J × DBA/NCrl) F1 hybrids. Six-week-old F2 progeny that were homozygous for the DBA/2J allele of *Fscn2* had 16 kHz ABR thresholds that were ~50 dB above those of heterozygotes or DBA/2NCrl-allele homozygotes (Fig. 3*e*). These results show that *Fscn2* genotypes strongly cosegregate with the hearing loss differences between these strains and that the DBA/2J allele conferring early onset hearing loss is recessive to the DBA/2NCrl allele.

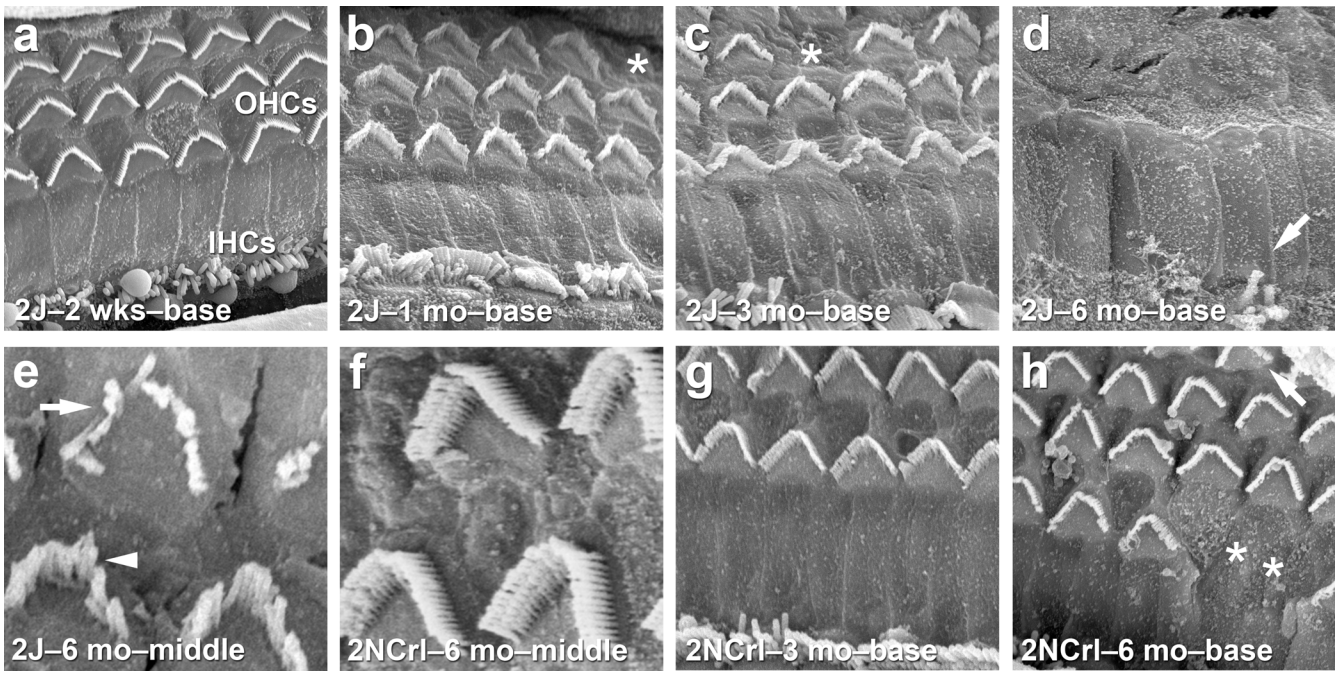

Figure 2. Rapid degeneration of cochlear hair cell bundles in DBA/2J mice. In the basal turn of the cochlea, bundles of outer hair cells (OHCs) and inner hair cells (IHCs) of DBA/2J mice (2J) appeared normal at 2 weeks of age (***a***), but at 1 month (***b***) and 3 months (***c***) of age, most OHC bundles already showed signs of degeneration, and some were missing (indicated by asterisks). By 6 months of age in the base (***d***), all OHCs were missing and the few remaining IHCs had degenerated bundles (indicated by arrow); in the middle turn (***e***), bundles were severely disheveled (arrowhead) and often had lost most rows of stereocilia (arrow). In contrast, all OHC and IHC bundles of the control DBA/2NCrl mice (2NCrl) at 3 months (***g***) and 6 months (***f***, ***h***) of age appeared normal, and only a few OHC bundles were missing (asterisks in ***h***); the bundles of the remaining OHCs appeared normal. A fourth row of OHCs was seen at frequent intervals throughout the length of the cochlea in both DBA/2J and DBA/2NCrl mice (indicated by arrow in ***h***). Panel widths: ***a–d***, ***g***, ***h***, 29 μm; ***e***, ***f***, 7.3 μm.

The wild-type allele of *Fscn2* rescues hearing loss

While supportive, cosegregation of *Fscn2* genotypes with hearing-loss differences between DBA/2J and other inbred strain mice does not prove causation as variants of other closely linked genes may be responsible for *ahl8*. We used a congenic-strain approach to further narrow the *ahl8* candidate gene region and to determine the isolated effect of *ahl8* on hearing loss. We generated two D2.B6-*ahl8* congenic lines containing differently sized regions of distal Chr 11 derived from C57BL/6J in an otherwise DBA/2J genome, both containing the *Fscn2* gene (Fig. 4*a*). Mice heterozygous for either congenic region retained normal hearing at the 2 month test age, whereas their DBA/2J littermates exhibited profound hearing loss (Fig. 4*b*,*c*). The line with the smallest segment of B6-derived Chr 11, which was only ~3 Mb, had the same effect as the line with the larger (26 Mb) segment. These results confirmed the recessive nature of the DBA/2J allele and showed that its full effect can be explained by genes within the small 3 Mb distal end of Chr 11. Notably, purified hair bundles contain none of the protein products of the ~100 genes in this region, except for FSCN2 and γ-actin (Shin et al., 2007; J.-B. Shin and P. G. Gillespie, unpublished data).

Although D2.B6-*ahl8* congenic line mice had ABR thresholds equivalent to C57BL/6J mice for click, 8 kHz, and 16 kHz auditory stimuli at the 2 month test age, their 32 kHz thresholds were significantly higher than those of C57BL/6J mice (Fig. 4*b*,*c*). These results suggest that there are other genetic differences between DBA/2J and C57BL/6J mice in addition to *ahl* (which they both carry) and *ahl8* that contribute to their different hearing loss profiles.

To provide definitive evidence that *Fscn2* underlies *ahl8*, we undertook a transgenic rescue approach. We produced two positive lines of transgenic mice from multiple DNA microinjections of a 178 kb C57BL/6J-derived BAC (RP24-180N9) containing *Fscn2* into DBA/2J embryos (Fig. 4*d*). This BAC was chosen because it contains the entire *Fscn2* gene and regulatory regions but does not include the closely linked gene for cytoplasmic γ-actin (*Actg1*), which, although it showed no nonsynonymous or splice site sequence variants in DBA/2J DNA, was still considered a possible candidate gene for *ahl8* because it has been shown to underlie progressive hearing loss in humans (Zhu et al., 2003) and mice (Belyantseva et al., 2009). Only one of the two BAC transgenic lines had detectable *Fscn2* transgene expression (Fig. 4*e*). Mice heterozygous for this expressed transgene (line 2) have significantly diminished hearing loss compared with nontransgenic DBA/2J littermates at 1 month of age (Fig. 4*g*). Mice heterozygous for the nonexpressed transgene (line 1) did not show this effect (Fig. 4*f*).

Although nine additional named genes are located in the 178 kb genomic region corresponding to BAC RP24-180N9 (Chr 11: 120221368–120399719, Build m37), analysis of high quality multifold resequencing data from the Welcome Trust Sanger Mouse Genomes Project (http://www.sanger.ac.uk/resources/mouse/genomes/) revealed that the *Fscn2* SNP (at position 120223348) is the only protein-coding sequence difference between DBA2J and C57BL/6J DNA in this region. There are no splice site, frameshift, or stop codon sequence differences and only one nucleotide difference in the 5′ UTR of the ADP-ribosylation factor-like 16 gene (*Arl16*; at position 120328095) and one nucleotide difference in the 3′ UTR of the HGF-regulated tyrosine kinase substrate gene (*Hgs*; at position 120344807). All other nucleotide sequence differences occur within intronic or intergenic regions. These results therefore demonstrate that the *Fscn2* mutation causes the early-onset, progressive hearing loss ascribed to *ahl8*.

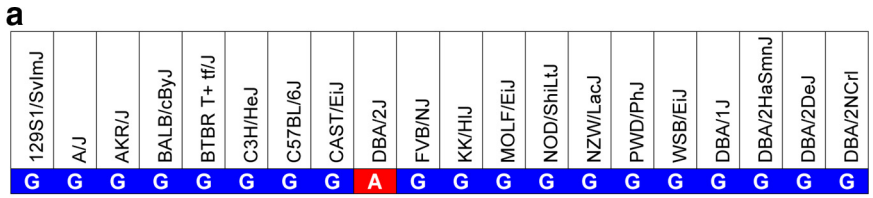

b

Protein	Genbank	Res.	Amino acid sequence
FSCN2 DBA/2J	strain SNP	90-129	FLVLPQPDGRWVLQSEPHG**H**FFGGIEDRLSCFATAISPAE
FSCN2 mouse	NP_766390	90-129	FLVLPQPDGRWVLQSEPHG**R**FFGGIEDRLSCFATAISPAE
FSCN2 rat	NP_001100542	90-129	FLVLPQPDGRWVLQSEPHG**R**FFGGVEDRLSCFATAISPAE
FSCN2 human	NP_036550	90-129	FLVLPQPDGRWVLRSEPHG**R**FFGGTEDQLSCFATAVSPAE
FSCN2 cow	NP_788806	90-129	FLVLPQPDGRWVLQSEPHG**R**FFGGTEDQLSCFATAITPAE
FSCN2 dog	XP_540481	90-129	FLVLPQPDGRWVLRSEPHG**R**FFGGTEDRLSCFATAISPAE
FSCN2 chicken	GU907099	89-128	FSIITQSDGRWALQSAPHR**R**FFGGREDRLSCFAPSITEGE
FSCN2 *Xenopus*	NP_001093724	90-129	FTISAQSDGRWALQSDPHK**R**FFGGSVDMLSCFAQTITETE
FSCN2a zebrafish	NP_001116988.1	88-127	FLIVMQSDGRWALQSEPYL**R**YFGGSEEYLSCFAQTIGESE
FSCN2b zebrafish	ACB72459	88-127	FLIVAQSDGRWALQSETYL**R**FFGGSEDYLSCFAQTIGEAE
FSCN1 mouse	NP_032010	91-130	FLVVAHDDGRWSLQSEAHR**R**YFGGTEDRLSCFAQSVSPAE
FSCN1 rat	NP_001094276	91-130	FLVVAHDDGRWSLQSEAHR**R**YFGGTEDRLSCFAQSVSPAE
FSCN1 human	NP_003079	91-130	FLIVAHDDGRWSLQSEAHR**R**YFGGTEDRLSCFAQTVSPAE
FSCN1 cow	NP_001030217	91-130	FLIVAHDDGRWSLQSEVHR**R**YFGGTEDRLSCFAQTVSPAE
FSCN1 dog	XP_546998	75-114	FLIVAHDDGRWSLQSEAHR**R**YFGGTEDRLSCFAQTVSPAE
FSCN1 chicken	GU952796	89-128	FLVVAHGDGRWSLQSEPHR**R**FFGGTEDRLSCFAPSVSPAE
FSCN1 *Xenopus*	NP_989128	83-122	FLVSAQGDGRWALQSEAYG**R**YFGGSEDRISCFSPSVSPAE
FSCN1 zebrafish	NP_001070028.1	89-128	FIITAHDDGRWSLQSEPHK**R**YLGGTEDRITCFAQTISIAE
FSCN3 mouse	NP_062515	95-134	FLLRFHRNGKWTLQCIISG**R**YLESDGEDVFCNSRVLSAYH
FSCN3 rat	NP_001004232	95-134	FLLRFHRNGKWTLQCIISG**R**YLESDGQDVFCNSRVLSAYH
FSCN3 human	NP_065102	95-134	FLLRFHRNSKWTLQCLISG**R**YLESNGKDVFCTSHVLSAYH
FSCN3 cow	NP_001069011	95-134	FLIRFHRNGQWTLQCIISG**R**YLESDGEDVFCTSRVLSAYH
FSCN3 pig	ABC54733	95-134	FLLRFHRNGKWTLQCIISG**R**YLESDGEDVFCTSRVLSAYH
FSCN pufferfish	CAG00222	73-112	FLIVPQSDGRWALQSEPYL**R**YFGGSADYLSCFAQAIGEQE
FSCN catshark	AAS49597	45-84	FLIVAHDDGRWSLQSEPHK**R**YFGGTEDRLTCFAQTISVAE
FSCN lungfish	AAS49529	54-93	FIIIAHDDGRXSLQSETHK**R**YFGGTEDRISCFAQTISVAE

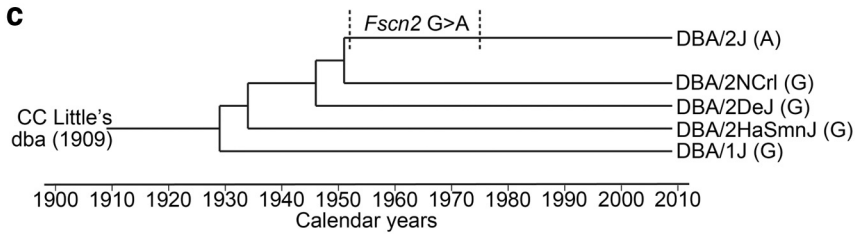

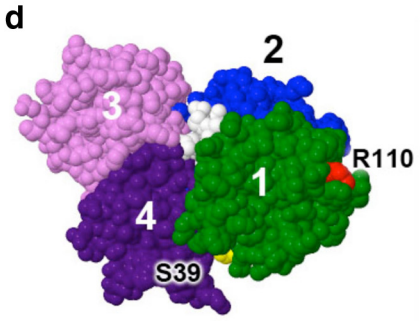

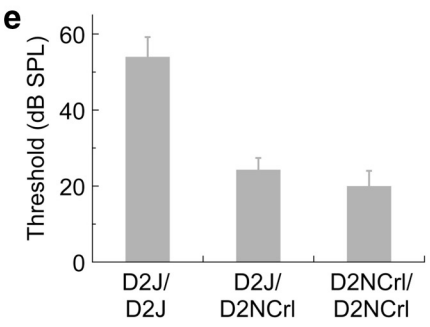

Figure 3. A SNP variant within the *Fscn2* gene is unique to the DBA/2J strain and changes a highly conserved amino acid. ***a***, Nucleotide variation among 20 inbred mouse strains for the rs26996001 SNP, which is located within exon 1 of the *Fscn2* gene. DBA/2J is the only strain examined with an adenine (A) at this position; all other strains have guanine (G). The G to A nucleotide substitution causes an amino acid change from arginine (R) to histidine (H) at position 109 of the mouse FSCN2 protein (NP_766390). ***b***, Evolutionary conservation of the FSCN2 arginine (R) residue that is mutated in DBA/2J mice. This residue (highlighted in blue) is conserved in fascin proteins of all mammalian species examined, as well as fascins of other vertebrate species. ***c***, Genealogy of DBA-related inbred mouse strains and their association with the *Fscn2* SNP. All are direct descendants of the original dba strain developed by C. C. Little in 1909. Shown are the approximate dates when these DBA-related inbred strains were separated from one another (Bailey, 1978; Zylstra et al., 2003). DBA/2J is the only strain with the G>A missense mutation in *Fscn2*; this mutation occurred sometime between 1951 and 1975, as deduced from archived DNA samples of DBA/2J strain mice. ***d***, Molecular model of FSCN1 (Protein Databank Structure 1DFC) showing the β-trefoil domains (1–4), the regulatory phosphorylation target S39, and the predicted location of the R109 residue of FSCN2 (R110 in FSCN1) that is mutated in DBA/2J mice. ***e***, Hearing loss in F2 intercross progeny of (DBA/2J × DBA/2NCrl) F1 hybrids strongly associates with homozygosity for the DBA/2J allele of *Fscn2*. Shown are the average 16 kHz ABR thresholds and SEs for each of the three *Fscn2* genotypes of F2 mice: D2J/D2J (homozygous for the DBA/2J mutation, $n = 9$), D2J/D2NCrl (heterozygous for the mutation, $n = 7$), and D2NCrl/D2NCrl (homozygous for the wild-type DBA/2NCrl allele, $n = 5$), all tested at 6 weeks of age. The DBA/2J mutant allele appears recessive to the DBA/2NCrl wild-type allele.

Identification and quantitation of FSCN2 in hair bundles

Identification of *Fscn2* as the causative gene for *ahl8* indicates that *Fscn2*, which encodes a known actin crosslinker, is expressed in the inner ear. The prominence of actin filaments in hair bundles motivated us to use mass spectrometry to search for actin crosslinkers, and specifically FSCN2, in hair bundles purified from E20 chicken utricles (Gillespie and Hudspeth, 1991; Shin et al., 2007). Although FSCN2 was not detected in our previous experiments (Shin et al., 2007), no *FSCN2* gene was present in the Ensembl chicken genome database before release 43 (February, 2007). Release 43 and beyond contain a fragment of the FSCN2 gene, encoding the C-terminal ~25% of the protein. Although subsequent searches with later Ensembl databases identified FSCN2 as one of the most abundant bundle proteins, we wished to search our mass-spectrometry data using a database containing full-length FSCN2. Using a combination of degenerate-primer RT-PCR and EST database searches, we determined the full-length sequence of chicken FSCN2, which shares high identity with mouse and frog FSCN2 (Fig. 5*a*; supplemental Fig. 1, available at www.jneurosci.org as supplemental material). We substituted the FSCN2 sequence fragment in Ensembl release 53 with the full-length sequence and searched this database with product-ion (MS2) spectra from hair bundles. Many FSCN2 peptides were identified from MS2 spectra with very high confidence, often with nearly complete y- and b-ion series (Fig. 5*b*). In five mass spectrometry runs, each with bundles from 100 chicken utricles, we identified >1000 FSCN2 peptides, covering nearly the entire sequence (Fig. 5*c*).

We used intensity-weighted spectral counting (Shin et al., 2007; Griffin et al., 2010) to quantify hair-bundle FSCN2. Using this approach, actin accounted for

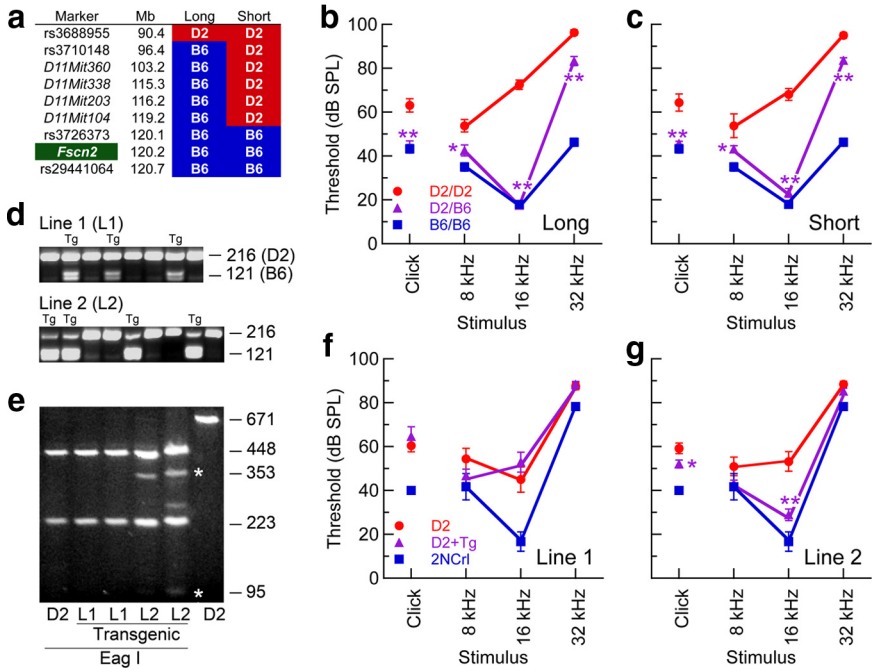

Figure 4. The wild-type C57BL/6J (B6) allele of *Fscn2* rescues hearing loss in congenic and transgenic lines of DBA/2J (D2) mice. ***a***, Markers defining the B6-derived distal Chr 11 regions for each of the two D2.B6 congenic lines, designated long (congenic region ~26 Mb) and short (congenic region ~3 Mb). ***b***, ***c***, ABR threshold means and SEs for heterozygous D2.B6 congenic line mice (D2/B6; long $n = 8$, short $n = 8$) and littermate D2 mice (D2/D2; long $n = 6$, short $n = 14$), tested at 2 months of age. Statistically significant ABR threshold differences between B6/D2 and D2/D2 mice are marked by asterisks: *$p < 0.05$; **$p < 0.001$. ABR thresholds of age-matched B6 mice (B6/B6; $n = 20$) are shown for comparison. ***d***, *Fscn2* transgene integration. The D2 mutation of *Fscn2* ablates an EagI restriction site that is present in the wild-type B6 allele, allowing detection of B6-derived *Fscn2* transgenes. After treatment with EagI, *Fscn2* PCR products of genomic DNA from mice with B6-derived transgenes include a diagnostic 121 bp fragment. The abundance of this B6-specific fragment, relative to the 216 bp endogenous D2 fragment, is much lower in line 1 than in line 2 transgenic mice. ***e***, *Fscn2* transgene expression. PCR primers specific to exons 1 and 2 of *Fscn2* were used to amplify a 671 bp product from cDNAs derived from brain and inner ear RNA. After digestion of this product with EagI, diagnostic B6-specific fragments of 353 and 95 bp could be detected in line 2 (L2) transgenic mice, but not in line 1 (L1) transgenic mice, which showed only the 448 and 223 bp fragments of D2 mice. ***f***, ***g***, ABR threshold means and SEs of DBA/2J mice with B6-derived *Fscn2* transgenes (D2+Tg; line 1 $n = 12$; line 2 $n = 19$) and their nontransgenic littermates (D2; line 1 $n = 10$, line 2 $n = 20$), tested at 1 month of age. ABR thresholds of age-matched DBA/2NCrl control mice (2NCrl; $n = 3$) are shown for comparisons. Statistically significant ABR threshold differences between D2+Tg and D2 mice are marked by asterisks: *$p < 0.05$; **$p < 0.001$.

55 ± 2% of the bundle protein on a molar basis, close to the 50–75% estimated from gel scanning (Gillespie and Hudspeth, 1991); by contrast, actin accounted for only ~10% of the total spectral counts. Chicken FSCN2 was present at a molar ratio of ~1:8 with actin (Fig. 5*d*), much higher than any other actin-crosslinking protein identified in the bundle preparation. At a crosslinker:actin ratio of ~1:75, PLS1 was the second-most abundant crosslinker (Fig. 5*d*); the crosslinkers FSCN1, plastin-2 (PLS2), PLS3, espin (ESPN), espin-like protein (ESPNL), and Xin-related protein 2 (XIRP2) were detected but were much less abundant.

We also adapted our methods for hair-bundle isolation and mass spectrometry to postnatal rat utricle bundles. Surprisingly, PLS1 was the most abundant actin crosslinker in P4–P6 rat bundles, present at a nearly fourfold higher concentration than FSCN2 (Fig. 5*d*), the second most abundant crosslinker. ESPNL and XIRP2 were present at low levels in rat bundles; by contrast, FSCN1, PLS2, PLS3, and ESPN were not detected.

We generated polyclonal rabbit antibodies specific for FSCN2 (Fig. 5*a*). Comparison of the immunoblot intensity for FSCN2 in hair bundles and whole epithelium with the corresponding total-protein stain showed that FSCN2 was strikingly enriched in bundles (Fig. 5*e–g*). In three experiments, the FSCN2:total protein ratio was 109-fold (±39) greater in bundles than in utricular epithelium.

Localization of FSCN2 and PLS1 in hair bundles

We used FSCN2 antibodies to localize the protein in the inner ears of several species. In E20 chicken utricles, FSCN2 immunoreactivity was specifically localized to hair bundles, particularly larger bundles (Fig. 6*a–c*), and was absent from smaller, likely immature hair cells (Fig. 6*c*, asterisk). In taller bundles, FSCN2 distribution was strikingly nonuniform; immunoreactivity was concentrated in the longer stereocilia and, in all stereocilia, was present in a gradient with the highest concentration at stereocilia tips (Fig. 6*b*,*c*). The last few rows of many hair bundles in the chick utricle had quite elongated stereocilia (Fig. 6*h*). Immunogold electron microscopy confirmed the FSCN2 localization and highlighted the concentration in the tallest stereocilia (Fig. 6*e*). FSCN2 was not only found in embryonic bundles; the protein was also localized at stereocilia tips in adult *Xenopus laevis* bundles (Fig. 6*d*).

PLS1 immunoreactivity, by contrast, was more apparent in the middle of chick hair bundles (Fig. 6*f*,*g*). Supporting this differential localization, the FSCN2:actin fluorescence ratio peaked at a more distal point of the bundle than did the PLS1:actin ratio (Fig. 6*g*); interestingly, neither crosslinker was abundant at stereocilia bases, even above tapers (Fig. 6*g*).

In mouse vestibular hair cells, FSCN2 expression was robust at all ages examined (P5, P10, P30); it was highly enriched in hair bundles, and also formed a gradient in stereocilia with the highest concentration at the tips (Fig. 7*g*; supplemental Fig. 2, available at www.jneurosci.org as supplemental material). By contrast, in mouse cochlear hair cells, we noted an age-dependent progression of FSCN2 expression. At P5 and earlier, little or no FSCN2 staining was observed in the organ of Corti (Fig. 7*a*). By P10, however, inner hair cells, including their bundles, showed strong FSCN2 immunoreactivity (Fig. 7*b*); FSCN2 was again concentrated at stereocilia tips, most prominently in the tallest row of stereocilia (Fig. 7*d*,*e*). In mature mice (P30), FSCN2 levels remained high in bundles of inner hair cells and also appeared in outer hair cells, including their bundles (Fig. 7*c*). FSCN2 localization in DBA/2J mice was similar temporally and spatially to that in WT mice (Fig. 7*f*), suggesting that the R109H mutation has little effect on FSCN2 trafficking or stability. In addition, the protein expression pattern of cytoplasmic γ-actin (ACTG1) in bundles was similar to that of FSCN2, with expression initiated between P5 and P10 and maintained after P10 (Fig. 7*h*).

Developmental regulation of *Fscn2* transcript levels

To determine whether developmental upregulation of FSCN2 in mouse cochlear hair cells was at the transcriptional or translational level, we isolated total RNA from cochleas of different ages

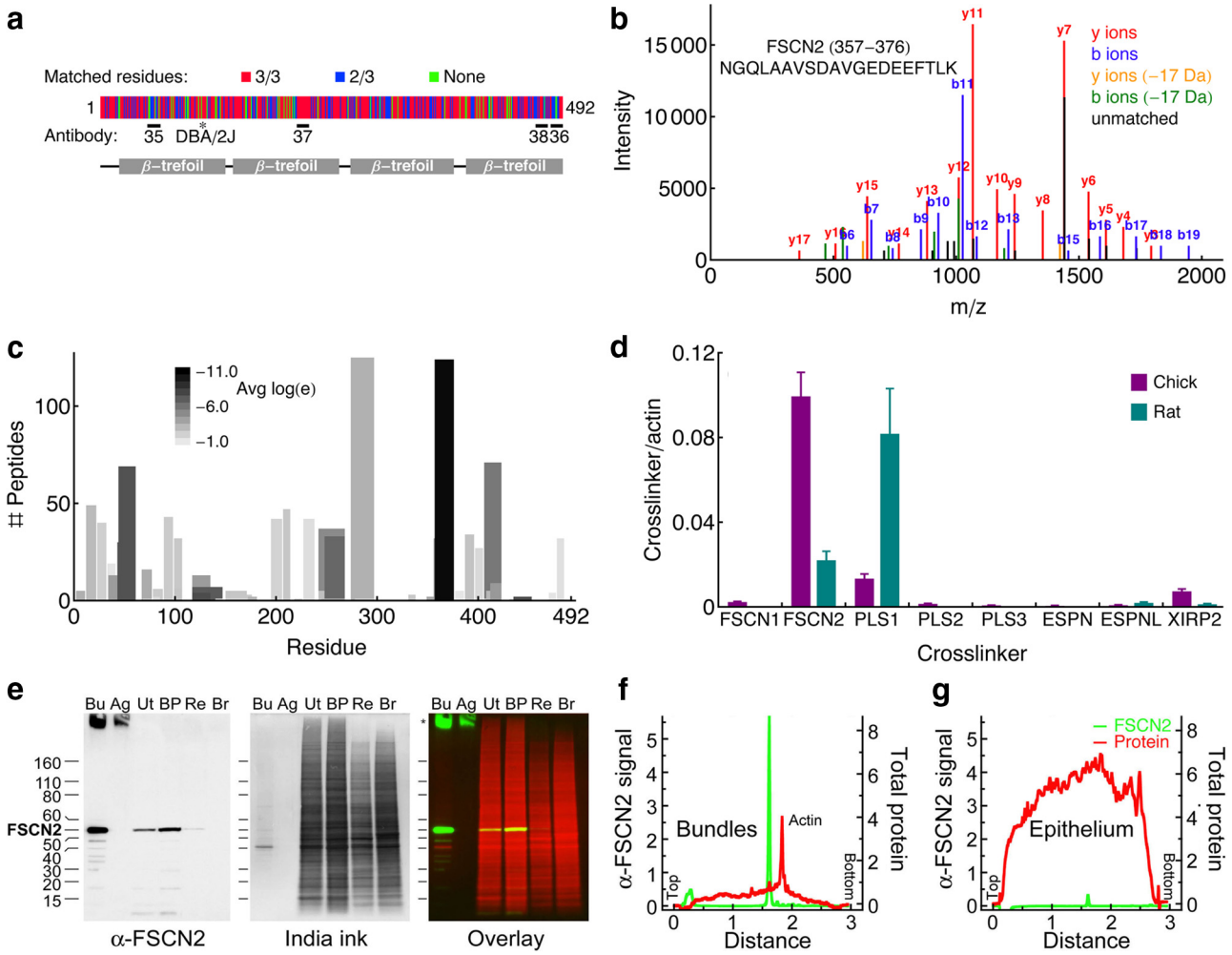

Figure 5. Identification and quantitation of FSCN2 in chicken vestibular stereocilia. ***a***, Structure of FSCN2 protein. Colors indicate identity of residues in three-way comparison of chicken, mouse, and *Xenopus* FSCN2. Peptides used for antibody generation are indicated by black bars and antibody numbers; the position of the mutation in DBA/2J is indicated with an asterisk. The positions of the four β-trefoil domains are indicated below. ***b***, Representative MS2 spectrum of a FSCN2 peptide identified by tandem mass spectrometry from a chicken hair bundle preparation. The intensity of peptide fragments, typically fragmented at peptide bonds during collision-induced dissociation, is plotted against the mass-to-charge ratio (*m/z*). Note the nearly complete y- and b-ion ladders, representing fragmentation sequentially at successive peptide bonds from the N and C termini. ***c***, Distribution of FSCN2 peptides identified by X! Tandem algorithm from hair bundles. The width of each bar indicates the length of the identified peptide, the position of the bar along the *x*-axis corresponds to its position in the FSCN2 sequence, the height of the bar indicates the number of identical peptides identified, and the color of the bar corresponds to log(*e*), the statistical significance for peptide identification, averaged over all identical peptides. Note that the peptide analyzed in ***b*** was one of those represented by the black bar at ~380 residues. ***d***, Crosslinker/actin abundance ratios in E20 chick and P5 rat vestibular hair bundles. ***e***, Immunoblot detection of FSCN2 in purified hair bundles with antibody 36. Bu, 100 ng of total hair-bundle protein; Ag, amount of agarose equivalent to that in bundles lane; Ut, 2 μg of peeled utricular epithelium; BP, 2 μg of peeled basilar papilla epithelium; Re, 1.5 μg of retina; and Br, 2 μg of total brain protein. ***f***, ***g***, Profile scans of bundle and utricular epithelium lanes from ***e***.

and performed quantitative PCR (qPCR) on reverse-transcribed RNA to measure transcript levels for *Fscn2*. In agreement with the immunolabeling results, the ratio of *Fscn2* transcript levels to those of *Gapdh* increased fivefold from P5 to P10 (Fig. 7*i*), when strong FSCN2 immunoreactivity was first visible in inner hair cells. *Fscn2* transcript levels reverted to the P5 level by P30, however, although FSCN2 protein levels remained high. *Pls1* transcripts increased approximately twofold at P10, then declined to the P5 level; by contrast, *Fscn1* transcripts continuously decreased in abundance from P5 to P30 (data not shown). *Actg1* (and *Actb*) were expressed at levels ~1000-fold higher than Fscn2 (Fig. 7*a*). Although we did not detect an age-dependent increase in *Actg1*/*Gapdh* transcript ratios (Fig. 7*i*), *Actg1* is expressed broadly in the cochlea (Belyantseva et al., 2009) and so any specific modulation in hair-cell levels would have been masked by the presence of *Actg1* transcripts elsewhere.

Discussion

A mutant allele of *Fscn2* causes rapid hearing loss in DBA/2J mice

We present multiple lines of evidence that a mutation in the *Fscn2* gene underlies the early onset progressive hearing loss of DBA/2J mice attributed to the *ahl8* locus: (1) the genetic map locations of *Fscn2* and *ahl8* coincide on distal Chr 11, (2) the *Fscn2* mutation is unique to the DBA/2J strain, and closely related DBA strains without this mutation do not exhibit early onset hearing loss and early hair bundle degeneration, (3) the amino acid altered by the *Fscn2* mutation in DBA/2J mice is highly conserved in homologous fascin proteins of all species examined, (4) FSCN2 is an abundant actin crosslinker in hair-cell stereocilia, (5) a 3 Mb B6-derived congenic segment of distal Chr 11 containing *Fscn2* lessens hearing loss in mice whose genomes are otherwise DBA/2J, and (6) expression of a B6-derived *Fscn2* transgene diminishes

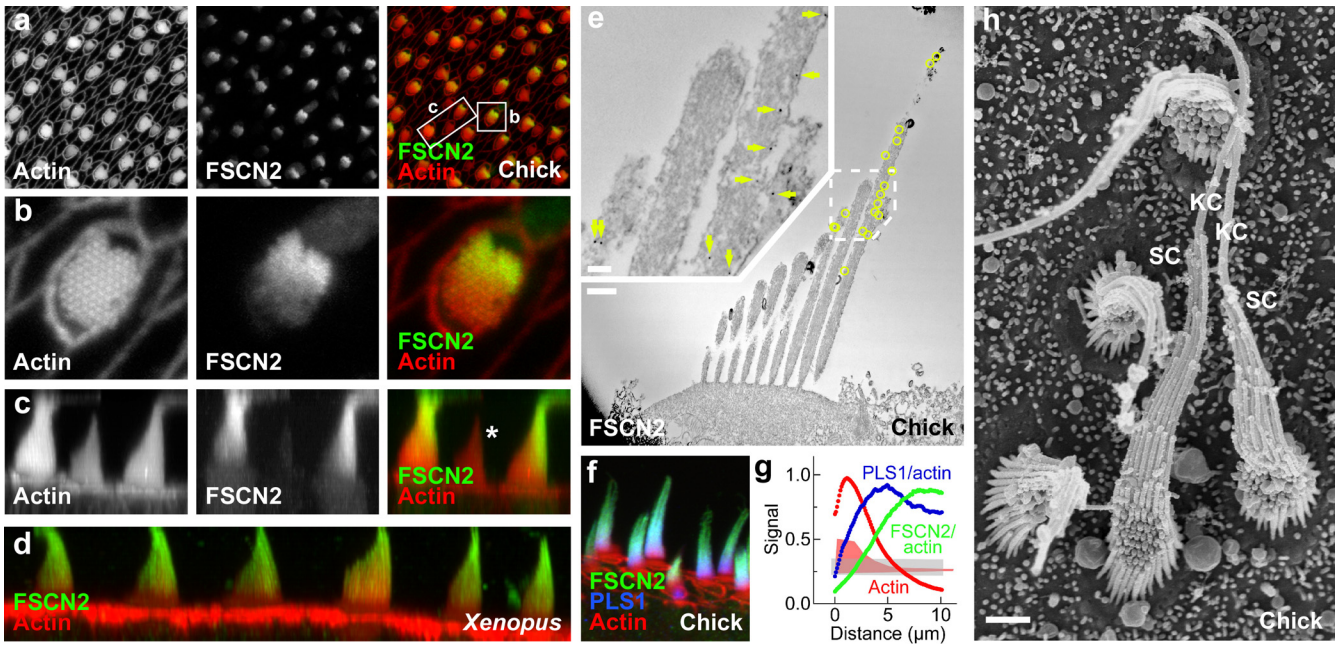

Figure 6. FSCN2 in chick and *Xenopus* hair bundles. ***a***, Low-power view of actin and FSCN2 in E20 chick utricle. Areas magnified in ***b*** and ***c*** are indicated. ***b***, High-power view of single bundle. Note high levels of FSCN2 in rows of tallest stereocilia, adjacent to kinocilium notch. ***c***, Reslice profile image of bundles showing localization of FSCN2 near stereocilia tips; tallest stereocilia are crushed against the coverslip. Note FSCN2 absence from a short, presumably immature bundle (asterisk). ***d***, Reslice profile image showing FSCN2 localization near tips of adult *Xenopus* saccule bundles. ***e***, Immunogold electron microscopy localization of FSCN2 in E20 chick utricle. All gold particles in micrograph are circled. Inset, magnification of region indicated with dashed lines. ***f***, Differential localization of crosslinkers in E20 chick utricle. Note concentration of FSCN2 toward tips and PLS1 in middle of bundles. Neither crosslinker is abundant at bundle base. ***g***. Quantitation of normalized actin signal, FSCN2/actin ratio, and PLS1/actin ratio in 14 cells from three utricle preparations. Diagram behind data depicts typical bundle morphology; gray box indicates region chosen for profile analysis. ***h***. Scanning electron micrograph showing typical chick utricle hair bundles; note the length of the tallest stereocilia. KC, Kinocilium; SC, stereocilia. Panel heights: ***a***, 52 μm; ***b***, 8 μm; ***c***, 12 μm; ***d***, 12 μm; ***f***, 32 μm. Scale bars: ***e***, 500 nm; ***e***, inset, 100 nm; ***h***, 1 μm.

hearing loss in DBA/2J mice. These results show that FSCN2 plays an important role in hair cells and compellingly demonstrate that the R109H mutation in FSCN2 compromises auditory function, presumably by altering FSCN2 crosslinking in stereocilia.

The R109 residue of FSCN2 is located on the surface of the first β-trefoil domain, opposite the regulatory residue S39 (Fig. 3*d*). While one actin-binding domain has been mapped to residues within β-trefoil domains 3 and 4 (Cant and Cooley, 1996; Ono et al., 1997), a second actin-binding domain—necessary for actin crosslinking—has yet to be localized. Indeed, R109 might plausibly participate in actin binding and bundling into fascicles, although additional experiments will be required to test that hypothesis.

Although the *Fscn2* gene was knocked out in mice without report of an auditory phenotype (Yokokura et al., 2005), progressive hearing loss cannot be readily detected in mice without specific assays. Interestingly, photoreceptor degeneration exhibited in *Fscn2*$^{-/-}$ mice was progressive with increasing age, consistent with the nature of the hearing loss in DBA/2J mice; DBA/2J mice show some age-related retinal degeneration, although it has been attributed to glaucoma (Schuettauf et al., 2004).

Function of FSCN2

FSCN2 is the most abundant actin crosslinking protein in chick vestibular hair bundles. In idealized fascicles of actin filaments, when all crosslinker sites are occupied, the packing density should be as high as one crosslinker per 4–5 actin monomers (Tilney et al., 1983), substantially more than the ratio seen by mass spectrometry (one FSCN2 per eight actins in chick). However, quantitation of FSCN2 in whole bundles underestimates its concentration at distal ends of long stereocilia, where it is concentrated; it might well be present at one FSCN2 per four actins in the upper third of these stereocilia.

FSCN2 expression in hair bundles is linked temporally with elongation of the tallest rows of stereocilia. For example, FSCN2 levels rise in bundles of mouse inner hair cells just when the tallest stereocilia grow substantially longer than their neighbors; 60% of their elongation occurs between P7 and P13 (Peng et al., 2009). By contrast, FSCN2 levels are low in bundles of outer hair cells, which do not elongate in the first week after birth and in fact shorten in the base (Lelli et al., 2009). Like in inner hair cells, FSCN2 is at highest levels in tall stereocilia of chick utricle bundles, particularly in maturing bundles that have already elongated substantially. FSCN2 might control stereocilia actin dynamics, stimulating growth of stereocilia by altering the balance between actin treadmilling and elongation; this hypothesis is consistent with experiments in zebrafish hair cells and tissue-culture cells, which showed that FSCN2 overexpression leads to elongated stereocilia and filopodia (McDermott et al., personal communication).

Alternatively, FSCN2 may play a structural role. The hair bundle's tallest stereocilia, which couple to overlying tectorial or otolithic structures, are often significantly longer than those in adjacent rows; they are nonetheless very rigid (Flock et al., 1977). Finite-element modeling shows that the stereocilium core's shear modulus to Young's modulus ratio must be high enough to prevent the tallest stereocilium from deforming (Cotton and Grant, 2000); FSCN2 might therefore stiffen these exposed stereocilia, enabling better force transmission to tip links. Indeed, members of the fascin family stiffen parallel actin fascicles in other organisms. In *Drosophila* bristles lacking fascin, actin filaments are poorly ordered and not extensively crosslinked; the resulting

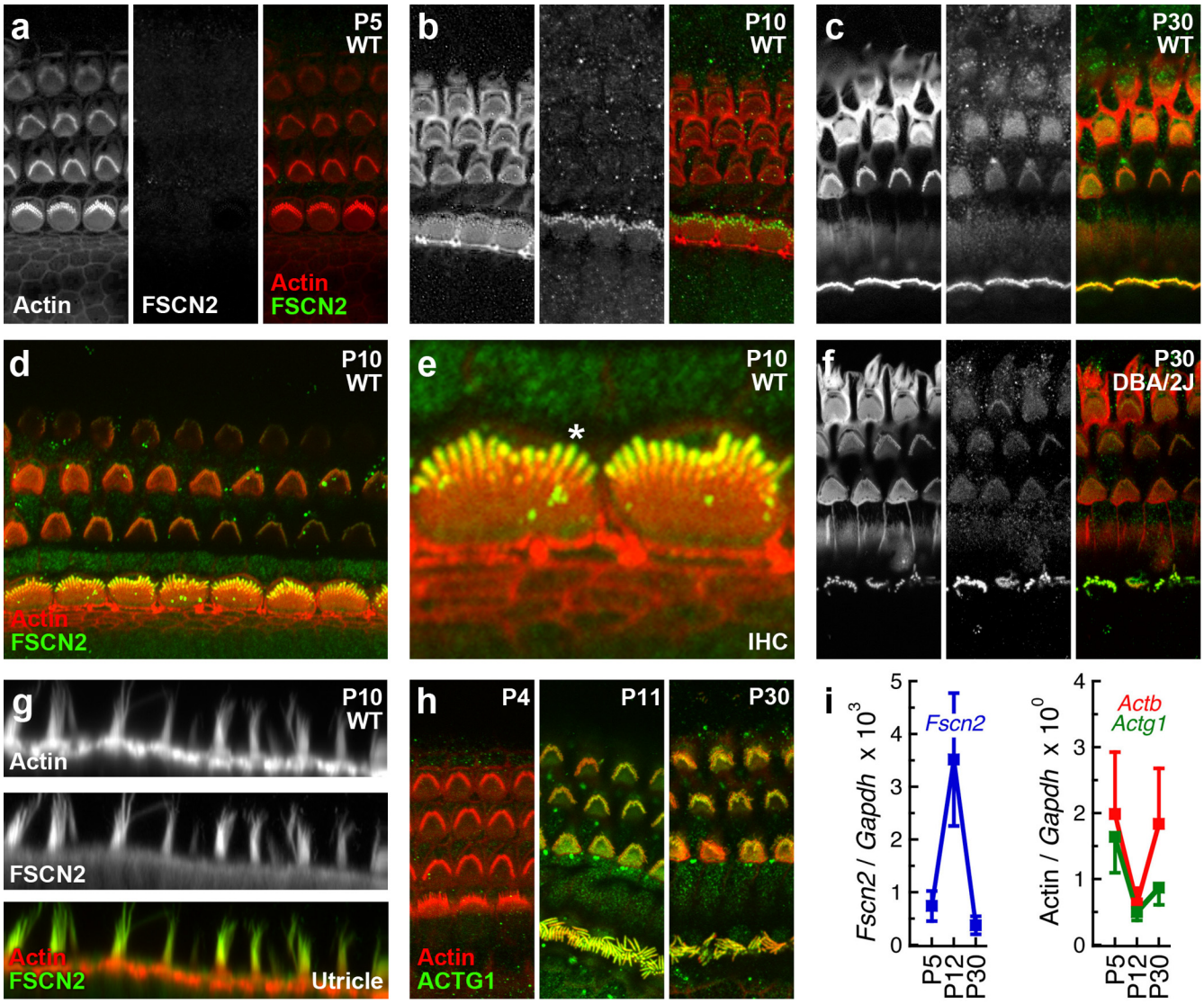

Figure 7. FSCN2 in mouse cochlea and vestibular system. ***a–c***, Developmental appearance of FSCN2 around P10 in bundles of inner hair cells and by P30 in bundles of outer hair cells. ***d***, FSCN2 in P10 cochlea; some labeling is seen in bundles of outer hair cells. The image is a maximum projection of 10 images, taken at 0.3 μm *z*-intervals. ***e***, Magnified view of two inner hair cell (IHC) bundles from ***d***. FSCN2 is primarily in the tallest stereocilia, near tips (asterisk). ***f***, Similar distribution of FSCN2 in P30 DBA/2J mice. ***g***, FSCN2 in mouse utricle hair bundles; note localization toward tips. The image is a *z*-projected (maximum) reslice image from a stack acquired axially through the utricular epithelium. ***h***, ACTG1 developmental appearance around P10 in mouse cochlea. ***i***, Quantitative RT-PCR showing elevation of FSCN2 transcripts around P10. No increase in *Actg1* or *Actb* transcript levels was seen. Panel heights: ***a–c***, ***f***, ***h***, 70 μm; ***d***, 60 μm; ***e***, ***g***, 19 μm.

bristles are much less stiff (Tilney and DeRosier, 2005). Filopodia lacking FSCN1 undergo buckling, suggesting that they are mechanically weak (Vignjevic et al., 2006). Thus, FSCN2 could be delivered to ends of long, exposed stereocilia to stiffen them.

Specific localization of FSCN2 to tall stereocilia could occur because the protein is specifically targeted there or because it preferentially incorporates into growing actin filaments. Actin in taller stereocilia treadmills faster than those in shorter ones, at least in young animals (Rzadzinska et al., 2004), so FSCN2 localization may simply report treadmilling rates. Reduced *Fscn2* expression at P30 while FSCN2 protein remains elevated suggests that this and other stereocilia proteins may be turned over at a rate lower than that seen earlier in development.

FSCN2 and PLS1 show opposing gradients in stereocilia, which can explain the observation that stereocilia in the frog sacculus are 0.7-fold narrower in diameter at their tips than near their bases in the ankle region (García et al., 1998); fascin crossbridges produce an actin filament spacing of 8.5 nm (DeRosier et al., 1977), while filaments are spaced 12 nm apart by plastin crossbridges (Volkmann et al., 2001), also a ratio of 0.7. One model for differential localization of two crosslinkers within the same actin fascicle suggests that FSCN2 expression late in hair-bundle development elongates actin filaments but slows treadmilling, quieting stereocilia actin dynamics and trapping PLS1 toward stereocilia bases. In a second model, FSCN2 is preferentially incorporated into treadmilling actin filaments, but dissociates rapidly and is replaced by PLS1 crossbridges; this mechanism is supported by experiments that show that FSCN1 crossbridges dissociate rapidly in filopodia (Vignjevic et al., 2006). Regardless, it is remarkable that stereocilia employ two primary actin crosslinkers, each of which can form tight, mechanically strong actin fascicles; that FSCN2 is essential for maintaining normal auditory function suggests either that it plays a special role that cannot be performed by PLS1 or that FSCN2-PLS1-actin fascicles have a composite behavior that cannot be matched with only one type of crosslinker (Tseng et al., 2002).

Degeneration of hair bundles in DBA/2J mice resembles degeneration seen in mice lacking γ-actin, which is required for stereocilia maintenance (Belyantseva et al., 2009). In both DBA/2J mice and γ-actin knock-out mice, hair bundles form normally but then progressively deteriorate, and by 16 weeks of age nearly all outer hair cell bundles show some missing or degraded stereocilia. Remarkably, *Fscn2* is only 13.0 kb from the γ-actin gene, *Actg1,* on mouse Chr 11 (Tubb et al., 2000) and undergoes upregulation in hair cells at the same time as does *Actg1*. Likewise, *FSCN2* is only 15.6 kb from *ACTG1* on human Chr 17. Nearby genes often share regulatory control (Michalak, 2008); because *Actb* and *Fscn1* are similarly closely linked on mouse Chr 5 (and *ACTB* and *FSCN1* on human Chr 7), we suggest that hair cells—as well as other cells—coordinately regulate these actin–fascin gene pairs for specific purposes.

Progressive hearing loss

Age-related, progressive hearing loss is influenced by many environmental and genetic factors, including variable exposures to noise, drugs and disease, genetic heterogeneity, allelic heterogeneity, and modifier loci (Johnson et al., 2006). Inbred mouse strains, which offer controlled genetics and minimized environmental variation, have shown that interactions of multiple alleles of the same gene or different genes can dramatically affect hearing acuity.

A particularly good example of such a genetic interaction is between *Cdh23*^{ahl} (Noben-Trauth et al., 2003) and *ahl8*, where rapid hearing loss in *ahl8/ahl8* mice is completely dependent on *Cdh23*^{ahl} homozygosity (Johnson et al., 2008). Mice that are homozygous for both *Cdh23*^{ahl} and *ahl8* display hearing loss that progresses much more rapidly than in mice that are heterozygous for one allele or the other (Johnson et al., 2008). Interestingly, *Cdh23*^{ahl} homozygosity sensitizes mice to the effects of other gene mutations, producing rapid hearing loss (Johnson et al., 2006).

These observations suggest that presbycusis might be more prevalent in individuals with multiple, relatively subtle, detrimental alleles encoding critical hair-bundle proteins such as FSCN2. Moreover, as *ACTG1* is close to *FSCN2*, *FSCN2* mutations may be responsible for those cases of DFNA20/26, a progressive dominant hearing loss disorder in humans, in which *ACTG1* mutations have not been found. Identification of *Fscn2* as the gene underlying the early hearing loss of DBA/2J mice will aid interpretation of results from the many studies that use this inbred strain. Moreover, that this mutation is unique to DBA/2J and not found in other DBA/2 designated strains provides a cautionary example of why genetic identity should not be assumed for like-named inbred strains from different sources. Finally, our results highlight the critical role that hair-bundle proteins play in hearing and show how a combination of proteomic and genetic approaches can be used to identify these proteins and determine their functional importance.

References

Bailey DW (1978) Sources of subline divergence and their relative importance for sublines of six major inbred strains of mice. In: Origins of inbred mice (Morse HC 3rd, ed), pp 197–215. New York: Academic.

Belyantseva IA, Perrin BJ, Sonnemann KJ, Zhu M, Stepanyan R, McGee J, Frolenkov GI, Walsh EJ, Friderici KH, Friedman TB, Ervasti JM (2009) Gamma-actin is required for cytoskeletal maintenance but not development. Proc Natl Acad Sci U S A 106:9703–9708.

Bretscher A, Weber K (1980) Fimbrin, a new microfilament-associated protein present in microvilli and other cell surface structures. J Cell Biol 86:335–340.

Cant K, Cooley L (1996) Single amino acid mutations in *Drosophila* fascin disrupt actin bundling function in vivo. Genetics 143:249–258.

Cotton JR, Grant JW (2000) A finite element method for mechanical response of hair cell ciliary bundles. J Biomech Eng 122:44–50.

Daudet N, Lebart MC (2002) Transient expression of the t-isoform of plastins/fimbrin in the stereocilia of developing auditory hair cells. Cell Motil Cytoskeleton 53:326–336.

DeRosier D, Mandelkow E, Silliman A (1977) Structure of actin-containing filaments from two types of non-muscle cells. J Mol Biol 113:679–695.

Flock A, Flock B, Murray E (1977) Studies on the sensory hairs of receptor cells in the inner ear. Acta Otolaryngol 83:85–91.

Flock A, Bretscher A, Weber K (1982) Immunohistochemical localization of several cytoskeletal proteins in inner ear sensory and supporting cells. Hear Res 7:75–89.

Furness DN, Hackney CM (1986) High-resolution scanning-electron microscopy of stereocilia using the osmium-thiocarbohydrazide coating technique. Hear Res 21:243–249.

García JA, Yee AG, Gillespie PG, Corey DP (1998) Localization of myosin-Ib near both ends of tip links in frog saccular hair cells. J Neurosci 18:8637–8647.

Gillespie PG, Hudspeth AJ (1991) High-purity isolation of bullfrog hair bundles and subcellular and topological localization of constituent proteins. J Cell Biol 112:625–640.

Gillespie PG, Müller U (2009) Mechanotransduction by hair cells: models, molecules, and mechanisms. Cell 139:33–44.

Griffin NM, Yu J, Long F, Oh P, Shore S, Li Y, Koziol JA, Schnitzer JE (2010) Label-free, normalized quantification of complex mass spectrometry data for proteomic analysis. Nat Biotechnol 28:83–89.

Grimm-Günter EM, Revenu C, Ramos S, Hurbain I, Smyth N, Ferrary E, Louvard D, Robine S, Rivero F (2009) Plastin 1 binds to keratin and is required for terminal web assembly in the intestinal epithelium. Mol Biol Cell 20:2549–2562.

Johnson KR, Zheng QY, Noben-Trauth K (2006) Strain background effects and genetic modifiers of hearing in mice. Brain Res 1091:79–88.

Johnson KR, Longo-Guess C, Gagnon LH, Yu H, Zheng QY (2008) A locus on distal chromosome 11 (ahl8) and its interaction with Cdh23 ahl underlie the early onset, age-related hearing loss of DBA/2J mice. Genomics 92:219–225.

Lelli A, Asai Y, Forge A, Holt JR, Géléoc GS (2009) Tonotopic gradient in the developmental acquisition of sensory transduction in outer hair cells of the mouse cochlea. J Neurophysiol 101:2961–2973.

Lin-Jones J, Burnside B (2007) Retina-specific protein fascin 2 is an actin cross-linker associated with actin bundles in photoreceptor inner segments and calycal processes. Invest Ophthalmol Vis Sci 48:1380–1388.

Liu XZ, Yan D (2007) Ageing and hearing loss. J Pathol 211:188–197.

Michalak P (2008) Coexpression, coregulation, and cofunctionality of neighboring genes in eukaryotic genomes. Genomics 91:243–248.

Noben-Trauth K, Johnson KR (2009) Inheritance patterns of progressive hearing loss in laboratory strains of mice. Brain Res 1277:42–51.

Noben-Trauth K, Zheng QY, Johnson KR (2003) Association of cadherin 23 with polygenic inheritance and genetic modification of sensorineural hearing loss. Nat Genet 35:21–23.

Ono S, Yamakita Y, Yamashiro S, Matsudaira PT, Gnarra JR, Obinata T, Matsumura F (1997) Identification of an actin binding region and a protein kinase C phosphorylation site on human fascin. J Biol Chem 272:2527–2533.

Peng AW, Belyantseva IA, Hsu PD, Friedman TB, Heller S (2009) Twinfilin 2 regulates actin filament lengths in cochlear stereocilia. J Neurosci 29:15083–15088.

Rzadzinska AK, Schneider ME, Davies C, Riordan GP, Kachar B (2004) An actin molecular treadmill and myosins maintain stereocilia functional architecture and self-renewal. J Cell Biol 164:887–897.

Rzadzinska A, Schneider M, Noben-Trauth K, Bartles JR, Kachar B (2005) Balanced levels of Espin are critical for stereociliary growth and length maintenance. Cell Motil Cytoskeleton 62:157–165.

Sakaguchi H, Tokita J, Müller U, Kachar B (2009) Tip links in hair cells: molecular composition and role in hearing loss. Curr Opin Otolaryngol Head Neck Surg 17:388–393.

Schirle M, Heurtier MA, Kuster B (2003) Profiling core proteomes of human cell lines by one-dimensional PAGE and liquid chromatography-tandem mass spectrometry. Mol Cell Proteomics 2:1297–1305.

Schuettauf F, Rejdak R, Walski M, Frontczak-Baniewicz M, Voelker M, Blatsios G, Shinoda K, Zagorski Z, Zrenner E, Grieb P (2004) Retinal neu-

rodegeneration in the DBA/2J mouse-a model for ocular hypertension. Acta Neuropathol 107:352–358.

Shin JB, Streijger F, Beynon A, Peters T, Gadzala L, McMillen D, Bystrom C, Van der Zee CE, Wallimann T, Gillespie PG (2007) Hair bundles are specialized for ATP delivery via creatine kinase. Neuron 53:371–386.

Tilney LG, DeRosier DJ (1986) Actin filaments, stereocilia, and hair cells of the bird cochlea. IV. How the actin filaments become organized in developing stereocilia and in the cuticular plate. Dev Biol 116:119–129.

Tilney LG, DeRosier DJ (2005) How to make a curved *Drosophila* bristle using straight actin bundles. Proc Natl Acad Sci U S A 102:18785–18792.

Tilney LG, Egelman EH, DeRosier DJ, Saunder JC (1983) Actin filaments, stereocilia, and hair cells of the bird cochlea. II. Packing of actin filaments in the stereocilia and in the cuticular plate and what happens to the organization when the stereocilia are bent. J Cell Biol 96:822–834.

Tseng Y, Schafer BW, Almo SC, Wirtz D (2002) Functional synergy of actin filament cross-linking proteins. J Biol Chem 277:25609–25616.

Tubb BE, Bardien-Kruger S, Kashork CD, Shaffer LG, Ramagli LS, Xu J, Siciliano MJ, Bryan J (2000) Characterization of human retinal fascin gene (FSCN2) at 17q25: close physical linkage of fascin and cytoplasmic actin genes. Genomics 65:146–156.

Vignjevic D, Kojima S, Aratyn Y, Danciu O, Svitkina T, Borisy GG (2006) Role of fascin in filopodial protrusion. J Cell Biol 174:863–875.

Volkmann N, DeRosier D, Matsudaira P, Hanein D (2001) An atomic model of actin filaments cross-linked by fimbrin and its implications for bundle assembly and function. J Cell Biol 153:947–956.

Yokokura S, Wada Y, Nakai S, Sato H, Yao R, Yamanaka H, Ito S, Sagara Y, Takahashi M, Nakamura Y, Tamai M, Noda T (2005) Targeted disruption of FSCN2 gene induces retinopathy in mice. Invest Ophthalmol Vis Sci 46:2905–2915.

Zheng L, Sekerková G, Vranich K, Tilney LG, Mugnaini E, Bartles JR (2000) The deaf jerker mouse has a mutation in the gene encoding the espin actin-bundling proteins of hair cell stereocilia and lacks espins. Cell 102:377–385.

Zheng QY, Johnson KR, Erway LC (1999) Assessment of hearing in 80 inbred strains of mice by ABR threshold analyses. Hear Res 130:94–107.

Zhu M, Yang T, Wei S, DeWan AT, Morell RJ, Elfenbein JL, Fisher RA, Leal SM, Smith RJ, Friderici KH (2003) Mutations in the gamma-actin gene (ACTG1) are associated with dominant progressive deafness (DFNA20/26). Am J Hum Genet 73:1082–1091.

Zylstra P, Franklin A, Hassan KA, Powell KL, Steele EJ, Blanden RV (2003) Molecular evolution of V(H)9 germline genes isolated from DBA, BALB, 129 and C57BL mouse strains and sublines. Immunogenetics 55:182–188.